Mixed finite elements for nonlocal elastic multilayered composite plate refined theories

Alberto Milazzo[a,*]

[a] *Department of Engineering, University of Palermo, Viale delle Scienze, Bld. 8, 90128 Palermo - Italy*

Abstract

A novel mixed finite element formulation for the layerwise analysis of nonlocal multilayered composite plates is presented. The finite elements are formulated starting from the weak form of a set of governing equations for the laminate layers that were deduced via the Reissner Mixed Variational Theorem. The primary variables, namely displacements and out-of-plane stresses, are expressed at layer level as through-the-thickness expansions of suitable selected functions with coefficients approximated by the finite element scheme. The through-the-thickness expansion order is considered as a free parameter. This way, finite elements for different refined higher order plate theories can be systematically developed by assembling the layers contributions associated with the variable expansion terms. These contributions are called fundamental nuclei and their definition is formally unique whatever the considered expansion order. The obtained finite elements inherently ensure stresses and displacements continuity at the layer interfaces and they allow to associate different values of the nonlocal parameter to the laminate layers. Standard 9-node and 16-node isoparametric, quadrilateral finite elements have been implemented to verify the viability of the proposed formulation. The obtained results compare favourably with literature solutions and highlights the characteristics of the approach. Original results are proposed also to serve as benchmarking data.

Keywords: Nonlocal elasticity, Refined plate theories, Reissner Mixed Variational Theorem, Mixed finite element, Laminated composites

1. Introduction

Small scale effects are observed in many engineering structural applications, which require careful modelling to avoid misjudgements in behaviour prediction and to ensure correct functionality. The

*Corresponding author. Tel.: +39 -91 23896748
Email address: alberto.milazzo@unipa.it (Alberto Milazzo)

Manuscript accepted on *to Composite Structures,* doi: https://doi.org/10.1016/j.compstruct.2020.112291

continuum theories based on hyperelastic constitutive relations do not account the small-scale effects and are generally unsuitable for the mechanical analysis of the micro and nanostructures. To overcome this scenario, modified continuum-based theories have been developed considering the small-scale effects[1, 2]. Among the approaches proposed in the literature, the Eringen's nonlocal elasticity model [3–5] has been recognized as very promising and then widely applied. It assumes that the stress at a point is a function of strains at all points in the continuum; this way, the small-scale effects are introduced through the constitutive equations, which involve a scale parameter depending on the material microstructure [6].

Based on the Eringen's nonlocal elasticity theory, several papers have been published for its application to beam-like structures (e.g. [7–10] and the reference cited therein). As regard modelling of plates, nonlocal Kirchhoff and Mindlin theories were formulated by Lu et al. [11] whereas the nonlocal third order shear deformation plate theory was proposed by Aghababei and Reddy [12]. Starting from these pioneering works, nonlocal plate theories have been applied to multilayered [13, 14] and smart plates [15–18]. The proposed two-dimensional theories for multilayered plates are usually formulated via the equivalent single layer (ESL) approach, which is not able to capture accurately the structural response characteristics associated with the variability in the material properties along the plate thickness. Additionally, the proposed nonlocal ESL theories consider a common value of the characteristic length for all the layers, despite this parameter can considerably vary for different materials [6]. Recently, in view of these observations, Milazzo et al. [19] proposed a layerwise formulation for nonlocal plates based on the Reissner Mixed Variational Theorem coupled with the primary variable expression axiomatically assumed according to the Carrera Unified Formulation [20, 21]. Accordingly, different higher order nonlocal multilayered plate theories have been systematically formulated and analysed.

However, the above-mentioned works are devoted to the theory development and assessment via closed form solutions for simple plates geometries, boundary conditions and loads. To deal with complex configurations, more general numerical methods are necessary. Therefore, finite element formulations for nonlocal behaviour of structures have then been proposed for beams [22–24], Kirchhoff's plates [22], Mindlin plates [25] and third order plate theories [14, 26, 27]. To the best of the author's knowledge finite elements for non local layerwise, high order plate theories have not been formulated yet.

In the present work, mixed finite elements for layerwise models of nonlocal multilayered plates are formulated resting on the approach proposed in Ref. [19]. To assess the approach features, 9-node

and 16-node isoparametric finite elements have been implemented for plate theories up to the fourth order. These have been studied and validated by comparison with closed form solutions available in the literature. Finally, an original configuration has been analysed to illustrate the proposed finite element potentiality and to provide possible benchmark solutions for future studies.

2. Multilayered plate models

Consider a multilayered plate with N layers, see Fig. 1. The plate is referred to a cartesian coordinate system with the x_3 axis directed along the thickness. The plate is subjected to the prescribed surface loads $\overline{\boldsymbol{q}}_t$ and $\overline{\boldsymbol{q}}_b$ applied on its top and bottom surfaces and to the prescribed tractions $\overline{\boldsymbol{t}}$ applied on its lateral surface.

In the following, the superscript $\langle k \rangle$ is used to label quantities referring to the k-th layer. The k-th layer has planform occupying the domain $\Omega^{\langle k \rangle} \equiv \Omega$ with boundary $\partial\Omega^{\langle k \rangle} \equiv \partial\Omega$ in the x_1x_2 plane and has constant thickness $h_k = z_k - z_{k-1}$ being z_{k-1} and z_k the x_3 coordinates of its bottom and top faces, respectively.

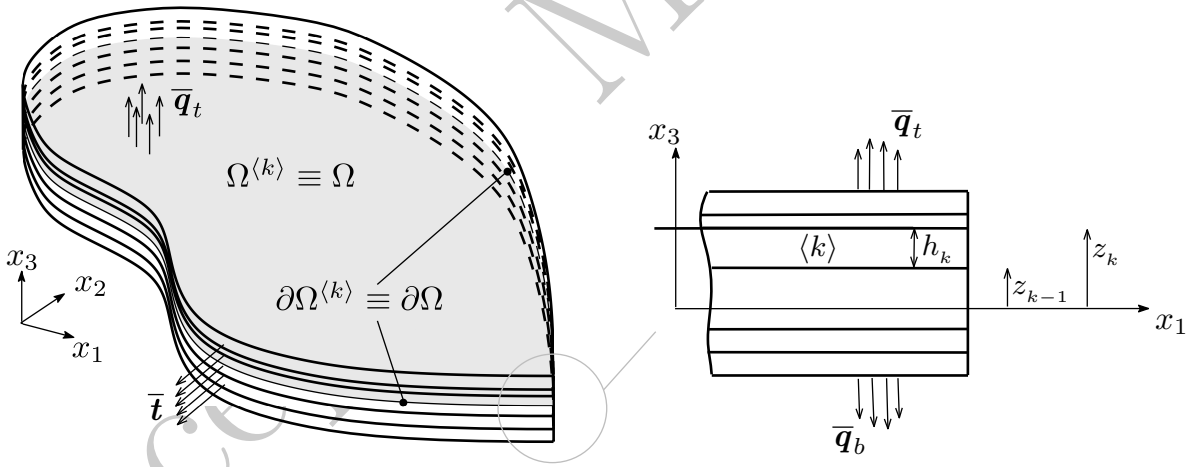

Figure 1: Plate scheme and geometrical definitions.

2.1. Layers constitutive law

The layers material behaviour is described via the Eringen's nonlocal elasticity model, which relates the local stresses $\tilde{\sigma}_{ij}$, to the nonlocal stresses σ_{ij} via the following differential relationship[5]

$$\mathcal{L}\sigma_{ij} = \tilde{\sigma}_{ij} \tag{1}$$

In the Eq. (1), the nonlocality operator $\mathcal{L}$ is defined as

$$\mathcal{L} = 1 - \ell \left(\frac{\partial^2}{\partial x_1^2} + \frac{\partial^2}{\partial x_2^2} \right) \tag{2}$$

where ℓ is the so-called nonlocal parameter, which depends on the material characteristic length [6].

The k-th layer constitutive equations are then suitably written as

$$\begin{Bmatrix} \mathcal{L}\boldsymbol{\sigma} \\ \mathcal{L}\boldsymbol{\tau} \end{Bmatrix} = \left[\begin{array}{c:c} \boldsymbol{C}_{pp} & \boldsymbol{C}_{pn} \\ \hdashline \boldsymbol{C}_{np} & \boldsymbol{C}_{nn} \end{array} \right] \begin{Bmatrix} \boldsymbol{\varepsilon} \\ \boldsymbol{\gamma} \end{Bmatrix} \tag{3}$$

where the stresses σ_{ij}, the normal strains ε_{ij} and the engineering shear strains γ_{ij} have been collected as $\boldsymbol{\sigma} = \begin{Bmatrix} \sigma_{11} & \sigma_{22} & \sigma_{12} \end{Bmatrix}^T$, $\boldsymbol{\tau} = \begin{Bmatrix} \sigma_{31} & \sigma_{32} & \sigma_{33} \end{Bmatrix}^T$, $\boldsymbol{\varepsilon} = \begin{Bmatrix} \varepsilon_{11} & \varepsilon_{22} & \gamma_{12} \end{Bmatrix}^T$ and $\boldsymbol{\gamma} = \begin{Bmatrix} \gamma_{31} & \gamma_{32} & \varepsilon_{33} \end{Bmatrix}^T$. The strain vectors $\boldsymbol{\varepsilon}$ and $\boldsymbol{\gamma}$ depend on the displacements through the following gradient equations

$$\boldsymbol{\varepsilon} = \boldsymbol{\partial}_p \boldsymbol{u} \tag{4a}$$

$$\boldsymbol{\gamma} = \boldsymbol{\partial}_n \boldsymbol{u} + \frac{\partial \boldsymbol{u}}{\partial x_3} \tag{4b}$$

where the operators $\boldsymbol{\partial}_p$ and $\boldsymbol{\partial}_n$ are defined in Appendix B. In Eq. (3), the $\boldsymbol{C}_{rs}$ matrices contain the stiffness elastic coefficients stemming from the classic Hooke's law.

2.2. Layer governing equations

According to the Carrera Unified Formulation [21], the displacements $\boldsymbol{u} = \begin{Bmatrix} u_1 & u_2 & u_3 \end{Bmatrix}^T$ and the out-of-plane stresses $\boldsymbol{\tau} = \begin{Bmatrix} \sigma_{31} & \sigma_{32} & \sigma_{33} \end{Bmatrix}^T$ are expressed at layer level as series expansions along the thickness:

$$\boldsymbol{u}^{\langle k \rangle}(x_1, x_2, x_3) = \sum_{\alpha=0}^{M} \boldsymbol{u}_\alpha^{\langle k \rangle}(x_1, x_2)\ F_\alpha^{\langle k \rangle}(x_3) \tag{5a}$$

$$\boldsymbol{\tau}^{\langle k \rangle}(x_1, x_2, x_3) = \sum_{\eta=0}^{M} \boldsymbol{\tau}_\eta^{\langle \kappa \rangle}(x_1, x_2)\ F_\eta^{\langle k \rangle}(x_3) \tag{5b}$$

where the definition of the thickness functions $F_\alpha^{\langle k \rangle}$ is given in Appendix A.

Considering $\boldsymbol{u}$ and $\boldsymbol{\tau}$ as primary variables and assuming that the essential boundary conditions, the gradient equations and the constitutive law are fulfilled, the governing equations for a layer within the laminate are obtained from the Reissner Mixed Variational Theorem (RMVT) [28–30], whose

variational statement for the k-th layer specializes as

$$\delta\Pi^{\langle k\rangle} = \int_\Omega \int_{h_k} \left[\delta {\boldsymbol{\varepsilon}_G^{\langle k\rangle}}^T \boldsymbol{\sigma}_C^{\langle k\rangle} + \delta {\boldsymbol{\gamma}_G^{\langle k\rangle}}^T \boldsymbol{\tau}_A^{\langle k\rangle} \right] dx_3 d\Omega + \int_\Omega \int_{h_k} \left[\delta {\boldsymbol{\tau}_A^{\langle k\rangle}}^T \left(\boldsymbol{\gamma}_G^{\langle k\rangle} - \boldsymbol{\gamma}_C^{\langle k\rangle} \right) \right] dx_3 d\Omega - \int_{\partial\Omega} \int_{h_k} \delta {\boldsymbol{u}_A^{\langle k\rangle}}^T \overline{\boldsymbol{t}}\, dx_3 d\partial\Omega - \int_\Omega \left[\left(\delta {\boldsymbol{u}_A^{\langle k\rangle}}^T \boldsymbol{\tau}_A^{\langle k\rangle} \right)\Big|_{z_k} - \left(\delta {\boldsymbol{u}_A^{\langle k\rangle}}^T \boldsymbol{\tau}_A^{\langle k\rangle} \right)\Big|_{z_{k-1}} \right] d\Omega = 0 \tag{6}$$

where δ denotes virtual variations and the notation $f|_z$ means evaluation of the function f at $x_3 = z$. In Eq. (6), the subscript "A" labels primary variables expressed via Eqs. (5) whereas the subscripts "G" and "C" refer to quantities evaluated via the gradient and the constitutive equations, respectively. Following the steps detailed in Refs. [31] and [19],the k-th layer governing equations are inferred. For $\alpha,\ \eta = 1, 2, \ldots, M$ they read as

$$\sum_{\beta=0}^{M} \left[\mathcal{I}_{\alpha\beta}^{\langle k\rangle} \boldsymbol{\partial}_p^T \boldsymbol{D}_{pp}^{\langle k\rangle} \boldsymbol{\partial}_p \right] \boldsymbol{u}_\beta^{\langle k\rangle} + \sum_{\lambda=0}^{M} \left[\mathcal{I}_{\alpha\lambda}^{\langle k\rangle} \boldsymbol{\partial}_p^T \boldsymbol{D}_{pn}^{\langle k\rangle} + \mathcal{I}_{\alpha\lambda}^{\langle k\rangle} \boldsymbol{\partial}_n^T - \mathcal{I}_{\alpha,3\lambda}^{\langle k\rangle} \right] \boldsymbol{\partial}_\ell^{\langle k\rangle} \boldsymbol{\tau}_\lambda^{\langle k\rangle} + \delta_{\alpha M}\, \boldsymbol{\partial}_\ell^{\langle k\rangle} \boldsymbol{\tau}_M^{\langle k\rangle} - \delta_{\alpha 0}\, \boldsymbol{\partial}_\ell^{\langle k\rangle} \boldsymbol{\tau}_0^{\langle k\rangle} = \boldsymbol{0} \qquad \text{in } \Omega^{\langle k\rangle} \tag{7a}$$

$$\sum_{\beta=0}^{M} \left[\mathcal{I}_{\eta\beta}^{\langle k\rangle} \boldsymbol{D}_{np}^{\langle k\rangle} \boldsymbol{\partial}_p - \mathcal{I}_{\eta\beta}^{\langle k\rangle}\ \boldsymbol{\partial}_n - \mathcal{I}_{\eta\beta,3}^{\langle k\rangle} \right] \boldsymbol{u}_\beta^{\langle k\rangle} + \sum_{\lambda=0}^{M} \left[\mathcal{I}_{\eta\lambda}^{\langle k\rangle} \boldsymbol{D}_{nn}^{\langle k\rangle} \right]\ \boldsymbol{\partial}_\ell^{\langle k\rangle} \boldsymbol{\tau}_\lambda^{\langle k\rangle} = \boldsymbol{0} \qquad \text{in } \Omega^{\langle k\rangle} \tag{7b}$$

$$\sum_{\beta=0}^{M} \left[\mathcal{I}_{\alpha\beta}^{\langle k\rangle} \widehat{\boldsymbol{\partial}}_p \boldsymbol{D}_{pp}^{\langle k\rangle} \boldsymbol{\partial}_p \right] \boldsymbol{u}_\beta^{\langle k\rangle} + \sum_{\lambda=0}^{M} \left[\mathcal{I}_{\alpha\lambda}^{\langle k\rangle} \widehat{\boldsymbol{\partial}}_p \boldsymbol{D}_{pn}^{\langle k\rangle} + \mathcal{I}_{\alpha\lambda}^{\langle k\rangle} \widehat{\boldsymbol{\partial}}_n \right] \boldsymbol{\partial}_\ell^{\langle k\rangle} \boldsymbol{\tau}_\lambda^{\langle k\rangle} - \overline{\boldsymbol{p}}_\alpha^{\langle k\rangle} = \boldsymbol{0} \qquad \text{in } \partial\Omega^{\langle k\rangle} \tag{7c}$$

where δ_{rs} denotes the Kronecker's delta. In Eqs. (7), the quantities inside square brackets are known as *fundamental nuclei*; they can be algorithmically evaluated with the same formal statements for any order of primary variables expansion. This allows to generate different high order layerwise plate theories systematically and straightforwardly [21]. The differential operators, coefficients and the material properties matrices appearing in the Eq. (7) are defined in Appendix B. Some remarks are appropriate in relation to Eq. (7). Observing that $\boldsymbol{\partial}_\ell^{\langle k\rangle} \boldsymbol{\tau}_\lambda^{\langle k\rangle} = \widetilde{\boldsymbol{\tau}}_\lambda^{\langle k\rangle}$, it appears that the layer governing equations could be written using the displacements $\boldsymbol{u}_\beta^{\langle k\rangle}$ and local out-of-plane stresses $\widetilde{\boldsymbol{\tau}}_\lambda^{\langle k\rangle}$ as primary variables. However, this option complicates the derivation of multilayered plate models, which are based on the coupling of the layers governing equations via the displacements and stresses continuity conditions at the layers interfaces (see Sec 2.3). Indeed, interface stress continuity physically involves the nonlocal stresses and not the local ones. So, assuming the nonlocal out-of-plane stresses as primary variables makes straightforward the enforcement of interface continuity especially when the layers exhibit different values of the nonlocal parameter ℓ. Moreover, because of the properties of the selected thickness functions (see Appendix A), $\boldsymbol{\tau}_0^{\langle k\rangle}$ and $\boldsymbol{\tau}_M^{\langle k\rangle}$ are the interlaminar stresses acting on

the bottom and top face of the ply. Additionally, for the first and last layer, $\boldsymbol{\tau}_0^{\langle 1\rangle}$ and $\boldsymbol{\tau}_M^{\langle N\rangle}$ correspond to the prescribed loads $\overline{\boldsymbol{q}}_b$ and $\overline{\boldsymbol{q}}_t$ applied on the plate bottom and top surfaces.

2.3. Multilayered plate governing equations

The governing equations for the multilayered plate are obtained by coupling the governing equations of the isolated layers, namely Eqs. (7) for $k=1,\,2,\,...,\,N$. This is accomplished through the enforcement of the interface continuity conditions. According to the properties of the selected thickness functions, they reduce to

$$\boldsymbol{u}_M^{\langle k\rangle} = \boldsymbol{u}_0^{\langle k+1\rangle} \qquad k=1,\,2,\,\ldots,\,(N-1) \tag{8a}$$

$$\boldsymbol{\tau}_M^{\langle k\rangle} = \boldsymbol{\tau}_0^{\langle k+1\rangle} \qquad k=1,\,2,\,\ldots,\,(N-1) \tag{8b}$$

3. FEM formulation

3.1. Finite element primary variable approximations

The in-plane behaviour of the primary variables is approximated by using two-dimensional finite elements [32]. For the k-th layer of the considered finite element, one writes

$$\boldsymbol{u}_\alpha^{\langle k\rangle}(x_1,x_2) = \boldsymbol{\mathcal{N}}_\alpha^{\langle k\rangle}\ \boldsymbol{\delta}_\alpha^{\langle k\rangle} \tag{9a}$$

$$\boldsymbol{\tau}_\eta^{\langle k\rangle}(x_1,x_2) = \boldsymbol{\mathcal{N}}_\eta^{\langle k\rangle}\ \boldsymbol{\vartheta}_\eta^{\langle k\rangle} \tag{9b}$$

where the vectors $\boldsymbol{\delta}_\alpha^{\langle k\rangle}$ and $\boldsymbol{\vartheta}_\eta^{\langle k\rangle}$ contains the nodal values of $\boldsymbol{u}_\alpha^{\langle k\rangle}$ and $\boldsymbol{\tau}_\eta^{\langle k\rangle}$, respectively, and $\boldsymbol{\mathcal{N}}^{\langle k\rangle}$ and $\boldsymbol{\mathcal{N}}_\eta^{\langle k\rangle}$ are matrices whose elements are the element shape functions.

The gradient relationships associated with Eqs (9), needed in the following to infer the finite element formulation, are written as

$$\boldsymbol{\partial}_p \boldsymbol{u}_\beta^{\langle k\rangle} = \left(\boldsymbol{\partial}_p\ \boldsymbol{\mathcal{N}}_\beta^{\langle k\rangle}\right)\boldsymbol{\delta}_\beta^{\langle k\rangle} = \boldsymbol{B}_{p\beta}^{\langle k\rangle}\boldsymbol{\delta}_\beta^{\langle k\rangle} \tag{10a}$$

$$\boldsymbol{\partial}_n \boldsymbol{u}_\beta^{\langle k\rangle} = \left(\boldsymbol{\partial}_n\ \boldsymbol{\mathcal{N}}_\beta^{\langle k\rangle}\right)\boldsymbol{\delta}_\beta^{\langle k\rangle} = \boldsymbol{B}_{n\alpha}^{\langle k\rangle}\boldsymbol{\delta}_\beta^{\langle k\rangle} \tag{10b}$$

$$\boldsymbol{\partial}_\ell^{\langle k\rangle} \boldsymbol{u}_\beta^{\langle k\rangle} = \left(\boldsymbol{\partial}_\ell^{\langle k\rangle}\boldsymbol{\mathcal{N}}_\beta^{\langle k\rangle}\right)\boldsymbol{\delta}_\beta^{\langle k\rangle} = \boldsymbol{B}_{\ell\beta}^{\langle k\rangle}\boldsymbol{\delta}_\beta^{\langle k\rangle} \tag{10c}$$

$$\boldsymbol{\partial}_\ell^{\langle k\rangle} \boldsymbol{\tau}_\eta^{\langle k\rangle} = \left(\boldsymbol{\partial}_\ell^{\langle k\rangle}\boldsymbol{\mathcal{N}}_\eta^{\langle k\rangle}\right)\ \boldsymbol{\vartheta}_\eta^{\langle k\rangle} = \boldsymbol{\mathcal{H}}_\eta^{\langle k\rangle}\boldsymbol{\vartheta}_\eta^{\langle k\rangle} \tag{10d}$$

3.2. Finite element layer governing equations

The weak form of the layer governing equations, Eq (7), is obtained as

$$\begin{aligned}
&\int_{\Omega^{\langle k\rangle}} \Bigg\{ \sum_{\alpha=0}^{M} \delta \boldsymbol{u}_{\alpha}^{\langle k\rangle T} \Bigg[\sum_{\beta=0}^{M} \mathcal{I}_{\alpha\beta}^{\langle k\rangle} \boldsymbol{D}_{pp}^{\langle k\rangle} \boldsymbol{\partial}_p \boldsymbol{u}_{\beta}^{\langle k\rangle} + \sum_{\lambda=0}^{M} \left(\mathcal{I}_{\alpha\lambda}^{\langle k\rangle} \boldsymbol{D}_{pp}^{\langle k\rangle} + \mathcal{I}_{\alpha\lambda}^{\langle k\rangle} \boldsymbol{\partial}_n^T - \mathcal{I}_{\alpha_{,3}\lambda}^{\langle k\rangle} \right) \boldsymbol{\partial}_{\ell}^{\langle k\rangle} \boldsymbol{\tau}_{\lambda}^{\langle k\rangle} \Bigg] + \\
&\quad \sum_{\alpha=0}^{M} \delta \boldsymbol{u}_{\alpha}^{\langle k\rangle T} \Bigg[\delta_{\alpha M}\ \boldsymbol{\partial}_{\ell}^{\langle k\rangle} \boldsymbol{\tau}_{M}^{\langle k\rangle} - \delta_{\alpha 0}\ \boldsymbol{\partial}_{\ell}^{\langle k\rangle} \boldsymbol{\tau}_{0}^{\langle k\rangle} \Bigg] + \\
&\quad \sum_{\eta=0}^{M} \delta \boldsymbol{\tau}_{\eta}^{\langle k\rangle T} \Bigg[\sum_{\beta=0}^{M} \left(\mathcal{I}_{\eta\beta}^{\langle k\rangle} \boldsymbol{D}_{np}^{\langle k\rangle} \boldsymbol{\partial}_p - \mathcal{I}_{\eta\beta}^{\langle k\rangle} \boldsymbol{\partial}_n - \mathcal{I}_{\eta\beta_{,3}}^{\langle k\rangle} \right) \boldsymbol{u}_{\beta}^{\langle k\rangle} + \sum_{\lambda=0}^{M} \mathcal{I}_{\eta\lambda}^{\langle k\rangle} \boldsymbol{D}_{nn}^{\langle k\rangle} \boldsymbol{\partial}_{\ell}^{\langle k\rangle} \boldsymbol{\tau}_{\lambda}^{\langle k\rangle} \Bigg] \Bigg\} d\Omega - \\
&\int_{\partial\Omega^{\langle k\rangle}} \Bigg\{ \sum_{\alpha=0}^{M} \delta \boldsymbol{u}_{\alpha}^{\langle k\rangle T} \Bigg[\sum_{\beta=0}^{M} \mathcal{I}_{\alpha\beta}^{\langle k\rangle} \widehat{\boldsymbol{\partial}}_p \boldsymbol{D}_{pp}^{\langle k\rangle} \boldsymbol{\partial}_p \boldsymbol{u}_{\beta}^{\langle k\rangle} + \sum_{\lambda=0}^{M} \left(\mathcal{I}_{\alpha\lambda}^{\langle k\rangle} \widehat{\boldsymbol{\partial}}_p \boldsymbol{D}_{pn}^{\langle k\rangle} + \mathcal{I}_{\alpha\lambda}^{\langle k\rangle} \widehat{\boldsymbol{\partial}}_n \right) \boldsymbol{\partial}_{\ell}^{\langle k\rangle} \boldsymbol{\tau}_{\lambda}^{\langle k\rangle} - \overline{\boldsymbol{p}}_{\alpha}^{\langle k\rangle} \Bigg] \Bigg\} d\partial\Omega = 0
\end{aligned} \tag{11}$$

Integrating by parts, Eq. (11) becomes

$$\begin{aligned}
&\int_{\Omega^{\langle k\rangle}} \sum_{\alpha=0}^{M} \sum_{\beta=0}^{M} \left(\boldsymbol{\partial}_p \delta \boldsymbol{u}_{\alpha}^{\langle k\rangle} \right)^T \mathcal{I}_{\alpha\beta}^{\langle k\rangle} \boldsymbol{D}_{pp}^{\langle k\rangle} \boldsymbol{\partial}_p \boldsymbol{u}_{\beta}^{\langle k\rangle} d\Omega + \\
&\int_{\Omega^{\langle k\rangle}} \sum_{\alpha=0}^{M} \sum_{\lambda=0}^{M} \Bigg[\left(\boldsymbol{\partial}_p \delta \boldsymbol{u}_{\alpha}^{\langle k\rangle} \right)^T \mathcal{I}_{\alpha\lambda}^{\langle k\rangle} \boldsymbol{D}_{pn}^{\langle k\rangle} + \left(\boldsymbol{\partial}_n \delta \boldsymbol{u}_{\alpha}^{\langle k\rangle} \right)^T \mathcal{I}_{\alpha\lambda}^{\langle k\rangle} + \delta \boldsymbol{u}_{\alpha}^{\langle k\rangle T} \mathcal{I}_{\alpha_{,3}\lambda}^{\langle k\rangle} \Bigg] \boldsymbol{\partial}_{\ell}^{\langle k\rangle} \boldsymbol{\tau}_{\lambda}^{\langle k\rangle} d\Omega - \\
&\int_{\Omega^{\langle k\rangle}} \delta \boldsymbol{u}_{M}^{\langle k\rangle T} \boldsymbol{\partial}_{\ell}^{\langle k\rangle} \boldsymbol{\tau}_{M}^{\langle k\rangle} d\Omega + \int_{\Omega^{\langle k\rangle}} \delta \boldsymbol{u}_{0}^{\langle k\rangle T} \boldsymbol{\partial}_{\ell}^{\langle k\rangle} \boldsymbol{\tau}_{0}^{\langle k\rangle} d\Omega - \\
&\int_{\Omega^{\langle k\rangle}} \sum_{\eta=0}^{M} \sum_{\beta=0}^{M} \delta \boldsymbol{\tau}_{\eta}^{\langle k\rangle} \Bigg[\mathcal{I}_{\eta\beta}^{\langle k\rangle} \boldsymbol{D}_{np}^{\langle k\rangle} \boldsymbol{\partial}_p - \mathcal{I}_{\eta\beta}^{\langle k\rangle} \boldsymbol{\partial}_n - \mathcal{I}_{\eta\beta_{,3}}^{\langle k\rangle} \Bigg] \boldsymbol{u}_{\beta}^{\langle k\rangle} d\Omega - \\
&\int_{\Omega^{\langle k\rangle}} \sum_{\eta=0}^{M} \sum_{\lambda=0}^{M} \mathcal{I}_{\eta\lambda}^{\langle k\rangle} \delta \boldsymbol{\tau}_{\eta}^{\langle k\rangle} \boldsymbol{D}_{nn}^{\langle k\rangle} \boldsymbol{\partial}_{\ell}^{\langle k\rangle} \boldsymbol{\tau}_{\lambda}^{\langle k\rangle} d\Omega - \int_{\partial\Omega^{\langle k\rangle}} \sum_{\alpha=0}^{M} \delta \boldsymbol{u}_{\alpha}^{\langle k\rangle T} \overline{\boldsymbol{p}}_{\alpha}^{\langle k\rangle} d\partial\Omega = 0
\end{aligned} \tag{12}$$

By substituting the finite element approximations Eqs (9) and (10) into Eq. (12) and taking the stationarity condition of the resulting statement, the finite element governing equations for the k-th layer are inferred as

$$\sum_{\beta=0}^{M} {}_{u}^{u}\boldsymbol{k}_{\alpha\beta}^{\langle k\rangle} \boldsymbol{\delta}_{\beta}^{\langle k\rangle} + \sum_{\lambda=0}^{M} {}_{\tau}^{u}\boldsymbol{k}_{\alpha\lambda}^{\langle k\rangle} \boldsymbol{\vartheta}_{\lambda}^{\langle k\rangle} - \delta_{\alpha M}\ \overline{\boldsymbol{k}}_{MM}^{\langle k\rangle} \boldsymbol{\vartheta}_{M}^{\langle k\rangle} + \delta_{\alpha 0}\ \overline{\boldsymbol{k}}_{00}^{\langle k\rangle} \boldsymbol{\vartheta}_{0}^{\langle k\rangle} - \boldsymbol{f}_{\alpha}^{\langle k\rangle} = \boldsymbol{0} \qquad \alpha = 0, \ldots, M \tag{13a}$$

$$\sum_{\beta=0}^{M} {}_{u}^{\tau}\boldsymbol{k}_{\eta\beta}^{\langle k\rangle} \boldsymbol{\delta}_{\beta}^{\langle k\rangle} + \sum_{\lambda=0}^{M} {}_{\tau}^{\tau}\boldsymbol{k}_{\eta\lambda}^{\langle k\rangle} \boldsymbol{\vartheta}_{\lambda}^{\langle k\rangle} = \boldsymbol{0} \qquad \eta = 0, \ldots, M \tag{13b}$$

In Eq. (13) the finite element fundamental nuclei are defined as

$${}_{u}^{u}\boldsymbol{k}_{\alpha\beta}^{\langle k\rangle} = \mathcal{I}_{\alpha\beta}^{\langle k\rangle} \int_{\Omega^{\langle k\rangle}} \boldsymbol{B}_{p\alpha}^{\langle k\rangle T} \boldsymbol{D}_{pp}^{\langle k\rangle} \boldsymbol{B}_{p\beta}^{\langle k\rangle} d\Omega \tag{14a}$$

$$ {}^{u}_{\tau}\boldsymbol{k}^{\langle k\rangle}_{\alpha\lambda} = \int_{\Omega}^{\langle k\rangle} \left[\mathcal{I}^{\langle k\rangle}_{\alpha\lambda} \boldsymbol{B}_{p\alpha}^{\langle k\rangle T} \boldsymbol{D}^{\langle k\rangle}_{pn} + \mathcal{I}^{\langle k\rangle}_{\alpha\lambda} \boldsymbol{B}_{n\alpha}^{\langle k\rangle T} + \mathcal{I}^{\langle k\rangle}_{\alpha,3\lambda} \boldsymbol{\mathcal{N}}_{\alpha}^{\langle k\rangle T} \right] \boldsymbol{\mathcal{H}}^{\langle k\rangle}_{\lambda} d\Omega \tag{14b} $$

$$ {}^{\tau}_{u}\boldsymbol{k}^{\langle k\rangle}_{\eta\beta} = \int_{\Omega^{\langle k\rangle}} \boldsymbol{\mathcal{N}}_{\eta}^{\langle k\rangle T} \left[\mathcal{I}^{\langle k\rangle}_{\eta\beta} \boldsymbol{D}^{\langle k\rangle}_{np} \boldsymbol{B}^{\langle k\rangle}_{p\beta} - \mathcal{I}^{\langle k\rangle}_{\eta\beta} \boldsymbol{B}_{n\beta}^{\langle k\rangle} - \mathcal{I}^{\langle k\rangle}_{\eta\beta,3} \boldsymbol{\mathcal{N}}_{\beta} \right] d\Omega \tag{14c} $$

$$ {}^{\tau}_{\tau}\boldsymbol{k}^{\langle k\rangle}_{\eta\lambda} = \mathcal{I}^{\langle k\rangle}_{\eta\lambda} \int_{\Omega} \boldsymbol{\mathcal{N}}_{\eta}^{\langle k\rangle T} \boldsymbol{D}^{\langle k\rangle}_{nn} \boldsymbol{\mathcal{H}}^{\langle k\rangle}_{\lambda} d\Omega \tag{14d} $$

$$ \overline{\boldsymbol{k}}^{\langle k\rangle}_{MM} = \int_{\Omega^{\langle k\rangle}} \boldsymbol{\mathcal{N}}_{M}^{\langle k\rangle T} \boldsymbol{\mathcal{H}}^{\langle k\rangle}_{M} d\Omega \tag{14e} $$

$$ \overline{\boldsymbol{k}}^{\langle k\rangle}_{00} = \int_{\Omega^{\langle k\rangle}} \boldsymbol{\mathcal{N}}_{0}^{\langle k\rangle T} \boldsymbol{\mathcal{H}}^{\langle k\rangle}_{0} d\Omega \tag{14f} $$

$$ \boldsymbol{f}^{\langle k\rangle}_{\alpha} = \int_{\partial\Omega^{\langle k\rangle}} \boldsymbol{\mathcal{N}}_{\alpha}^{\langle k\rangle T} \overline{\boldsymbol{p}}^{\langle k\rangle}_{\alpha} d\partial\Omega \tag{14g} $$

It is remarked that the fundamental nuclei $\overline{\boldsymbol{k}}^{\langle k\rangle}_{MM}$ and $\overline{\boldsymbol{k}}^{\langle k\rangle}_{00}$ account for the tractions applied on the top and bottom faces of the layer, which correspond to the interlaminar stresses. For the layers with external faces ($k=1$ and $k=N$) the fundamental nuclei $\overline{\boldsymbol{k}}^{\langle N\rangle}_{MM}$ and $\overline{\boldsymbol{k}}^{\langle 1\rangle}_{00}$ provide the contribution of the prescribed loads $\overline{\boldsymbol{q}}_t$ and $\overline{\boldsymbol{q}}_b$ applied on the plate top and bottom surfaces, respectively.

3.3. Multilayered plate finite elements: along thickness assembly

The finite element equations for the multilayered plates are obtained by coupling those of the isolated layers via the interface displacements and stresses continuity, whose discretized form stems from Eq. (8) and read as

$$ \boldsymbol{\delta}^{\langle k\rangle}_{M} = \boldsymbol{\delta}^{\langle k+1\rangle}_{0} \qquad k=1,\,2,\,\ldots,\,(N-1) \tag{15a} $$

$$ \boldsymbol{\vartheta}^{\langle k\rangle}_{M} = \boldsymbol{\vartheta}^{\langle k+1\rangle}_{0} \qquad k=1,\,2,\,\ldots,\,(N-1) \tag{15b} $$

Additionally, for the applied surface loads the following relationships hold

$$ \boldsymbol{\vartheta}^{\langle 1\rangle}_{0} = \overline{\boldsymbol{q}}_b \tag{16a} $$

$$ \boldsymbol{\vartheta}^{\langle N\rangle}_{M} = \overline{\boldsymbol{q}}_t \tag{16b} $$

Introducing the element nodal unknowns vectors as

$$\boldsymbol{\Delta}^T = \left\{ \begin{array}{cccccc} \boldsymbol{\Delta}_0 = \boldsymbol{\delta}_0^{\langle 1 \rangle T} & \cdots & \boldsymbol{\Delta}_{\alpha+M(k-1)}{}^T = \boldsymbol{\delta}_\alpha^{\langle k \rangle T} & \cdots & \boldsymbol{\Delta}_{NM+1}^T = \boldsymbol{\delta}_M^{\langle N \rangle T} \end{array} \right\} \tag{17a}$$

$$\boldsymbol{\Theta}^T = \left\{ \begin{array}{cccccc} \boldsymbol{\Theta}_0 = \boldsymbol{\vartheta}_0^{\langle 1 \rangle T} & \cdots & \boldsymbol{\Theta}_{\eta+M(k-1)}{}^T = \boldsymbol{\vartheta}_\eta^{\langle k \rangle T} & \cdots & \boldsymbol{\Theta}_{NM+1}^T = \boldsymbol{\vartheta}_M^{\langle N \rangle T} \end{array} \right\} \tag{17b}$$

the plate finite element equations, namely Eqs. (13) and (15), are recast in the standard form as

$$\begin{bmatrix} {}_u^u\boldsymbol{K} & {}_\tau^u\boldsymbol{K} \\ {}_u^\tau\boldsymbol{K} & {}_\tau^\tau\boldsymbol{K} \end{bmatrix} \begin{Bmatrix} \boldsymbol{\Delta} \\ \boldsymbol{\Theta} \end{Bmatrix} = \begin{Bmatrix} \boldsymbol{F} \\ \boldsymbol{0} \end{Bmatrix} \tag{18}$$

The matrices involved in Eq. (18) are obtained from the fundamental nuclei via an assembly procedure stemming from Eqs (15). In particular the assembly follows the scheme described in the following relationship

$$ {}_s^r\boldsymbol{K} = \begin{bmatrix} {}_s^r\boldsymbol{k}_{00}^{\langle 1 \rangle} & \cdots & & & & & & & & & \\ \vdots & \ddots & & & & & & & & & \\ & & \left[{}_s^r\boldsymbol{k}_{MM}^{\langle k-2 \rangle} + {}_s^r\boldsymbol{k}_{00}^{\langle k-1 \rangle} - \chi\left(\overline{\boldsymbol{k}}_{MM}^{\langle k-2 \rangle} - \overline{\boldsymbol{k}}_{00}^{\langle k-1 \rangle} \right) \right] & \cdots & {}_s^r\boldsymbol{k}_{0\beta}^{\langle k-1 \rangle} & \cdots & {}_s^r\boldsymbol{k}_{0M}^{\langle k-1 \rangle} & & \\ & & \vdots & \ddots & \vdots & \vdots & \ddots & & \\ & & {}_s^r\boldsymbol{k}_{\alpha 0}^{\langle k-1 \rangle} & \cdots & {}_s^r\boldsymbol{k}_{\alpha\beta}^{\langle k-1 \rangle} & \cdots & {}_s^r\boldsymbol{k}_{\alpha M}^{\langle k-1 \rangle} & & \\ & & \vdots & \ddots & \vdots & \ddots & \vdots & & \\ & & {}_s^r\boldsymbol{k}_{M0}^{\langle k-1 \rangle} & \cdots & {}_s^r\boldsymbol{k}_{M\beta}^{\langle k-1 \rangle} & \cdots & \left[{}_s^r\boldsymbol{k}_{MM}^{\langle k-1 \rangle} + {}_s^r\boldsymbol{k}_{00}^{\langle k \rangle} - \chi\left(\overline{\boldsymbol{k}}_{MM}^{\langle k-1 \rangle} - \overline{\boldsymbol{k}}_{00}^{\langle k \rangle} \right) \right] & \cdots & {}_s^r\boldsymbol{k}_{0\beta}^{\langle k \rangle} & \cdots & {}_s^r\boldsymbol{k}_{0M}^{\langle k \rangle} \\ & & & & \vdots & \ddots & \vdots & \ddots & \vdots \\ & & & & {}_s^r\boldsymbol{k}_{\alpha 0}^{\langle k \rangle} & \cdots & {}_s^r\boldsymbol{k}_{\alpha\beta}^{\langle k \rangle} & \cdots & {}_s^r\boldsymbol{k}_{\alpha M}^{\langle k \rangle} \\ & & & & \vdots & \ddots & \vdots & \ddots & \vdots \\ & & & & {}_s^r\boldsymbol{k}_{M0}^{\langle k \rangle} & \cdots & {}_s^r\boldsymbol{k}_{M\beta}^{\langle k \rangle} & \cdots & \left[{}_s^r\boldsymbol{k}_{MM}^{\langle k \rangle} + {}_s^r\boldsymbol{k}_{00}^{\langle k+1 \rangle} - \chi\left(\overline{\boldsymbol{k}}_{MM}^{\langle k \rangle} - \overline{\boldsymbol{k}}_{00}^{\langle k+1 \rangle} \right) \right] \cdots \\ & & & & & & & & \ddots \quad \vdots \\ & & & & & & & & \cdots {}_s^r\boldsymbol{k}_{MM}^{\langle N \rangle} \end{bmatrix} \tag{19}$$

where $\chi = 1$ for $r = u$ and $s = \tau$ and $\chi = 0$ otherwise. Eventually, the right-hand-side vector is obtained as follows

$$\boldsymbol{F}^T = \left\{ \left(\boldsymbol{f}_0^{\langle 1 \rangle} + \overline{\boldsymbol{k}}_{00}^{\langle 1 \rangle} \overline{\boldsymbol{q}}_b \right)^T \quad \cdots \quad \boldsymbol{f}_M^{\langle k-1 \rangle T} \quad \boldsymbol{f}_0^{\langle k \rangle T} \quad \cdots \quad \left(\boldsymbol{f}_M^{\langle N \rangle} + \overline{\boldsymbol{k}}_{MM}^{\langle N \rangle} \overline{\boldsymbol{q}}_t \right)^T \right\} \tag{20}$$

Once the element equations have been established, standard assembly procedures are used to obtain the resolving system for the finite element discretized structures.

4. Results

To illustrate the capabilities of the proposed formulation and its characteristics, the 9-node and the 16-node isoparametric finite elements have been implemented. According to the established literature on isoparametric finite elements for plates [32], the element matrices have been computed using the selective reduced integration technique to contrast locking phenomena [33].

A [0/90/90/0] symmetric cross-ply, simply supported, square plate with side length $a = 10\,\text{nm}$ and thickness h is considered. The plate undergoes a transverse bisinusoidal load applied on its top surface with amplitude q_0. The layers exhibit the following material properties

$$\frac{E_1}{E_2} = 25; \quad \frac{G_{12}}{E_2} = \frac{G_{13}}{E_2} = 0.5; \quad \frac{G_{23}}{E_2} = 0.2; \quad \nu_{12} = \nu_{13} = \nu_{23} = 0.25 \tag{21}$$

being E_i, G_{ij} and ν_{ij} the Young's moduli, the shear moduli and the Poisson's coefficients, respectively. Analyses have been carried out assuming the same nonlocal parameter ℓ for all the layers and varying its value from 0 (local behaviour) to 5. Different plate theories are considered varying the order of the primary variables thickness expansion up to the fourth. Each theory is labelled by the acronym LWn_ℓ where n denotes the order of the employed expansion and ℓ indicates the value of the nonlocal parameter.

First, convergence studies have been performed by using $m \times m$ regular meshes of the 9-node and 16-node elements. The selective reduced integration technique was used to compute the elements matrices. Tables 1 and 2 illustrate the convergence study for the 9-node and 16-node finite elements, respectively. They list the results for the nondimensional transverse displacement $\bar{u}_3 = 100 u_3 E_2 h^3 / q_0 a^4$ at the plate center and their comparison with literature solutions [14, 19]. Two different plate thickness ratio a/h have been investigated. The results evidence good convergence characteristics for all the considered plate theories and for the different values of the nonlocal parameter ℓ.

To assess the formulation accuracy, the through-the-thickness distributions of displacements and stresses at the point with in-plane coordinates $(a/4, a/4)$ have been investigated. Figs. 2 and 3 show the through-the-thickness distributions of the u_1 and u_3 displacement components of the plate with $a/h = 10$, obtained using a 8×8 mesh of 9-node elements and a 5×5 mesh of 16-node elements, respectively; the two employed meshes have been chosen so as to obtain models with comparable numbers of degrees of freedom. The results evidence a very good agreement between the present and the closed form solution of Ref. [19], suggesting that the displacement field is captured with high

Table 1: Convergence analysis for the 9-node isoparametric finite element: nondimensional transverse displacement $\bar{u}_3 = 100 u_3 E_2 h^3 / q_0 a^4$ at the plate center.

			Mesh					
a/h	ℓ	Plate theory	4×4	6×6	8×8	10×10	Ref. [19]	Ref. [14]
10	0	$LW1$	0.744	0.742	0.742	0.741	0.740	0.715
		$LW2$	0.739	0.737	0.737	0.736	0.736	
		$LW3$	0.739	0.737	0.737	0.736	0.736	
		$LW4$	0.739	0.737	0.737	0.736	0.736	
	1	$LW1$	0.889	0.887	0.887	0.887	0.887	0.856
		$LW2$	0.883	0.881	0.881	0.881	0.881	
		$LW3$	0.883	0.881	0.881	0.881	0.881	
		$LW4$	0.883	0.881	0.881	0.881	0.881	
	3	$LW1$	1.181	1.179	1.179	1.179	1.179	1.139
		$LW2$	1.173	1.172	1.172	1.171	1.171	
		$LW3$	1.173	1.172	1.172	1.171	1.171	
		$LW4$	1.173	1.172	1.172	1.171	1.171	
	5	$LW1$	1.473	1.472	1.471	1.471	1.471	1.421
		$LW2$	1.464	1.462	1.462	1.462	1.462	
		$LW3$	1.464	1.462	1.462	1.462	1.462	
		$LW4$	1.464	1.462	1.462	1.462	1.462	
20	0	$LW1$	0.515	0.514	0.514	0.514	0.514	0.506
		$LW2$	0.514	0.513	0.513	0.513	0.513	
		$LW3$	0.514	0.513	0.513	0.513	0.513	
		$LW4$	0.514	0.513	0.513	0.513	0.513	
	1	$LW1$	0.616	0.615	0.615	0.615	0.615	0.606
		$LW2$	0.615	0.614	0.614	0.614	0.614	
		$LW3$	0.615	0.614	0.614	0.614	0.614	
		$LW4$	0.615	0.614	0.614	0.614	0.614	
	3	$LW1$	0.819	0.818	0.818	0.818	0.818	0.806
		$LW2$	0.817	0.817	0.816	0.816	0.816	
		$LW3$	0.817	0.817	0.816	0.816	0.816	
		$LW4$	0.817	0.817	0.816	0.816	0.816	
	5	$LW1$	1.022	1.021	1.021	1.021	1.021	1.006
		$LW2$	1.020	1.019	1.019	1.019	1.019	
		$LW3$	1.020	1.019	1.019	1.019	1.019	
		$LW4$	1.020	1.019	1.019	1.019	1.019	

Table 2: Convergence analysis for the 16-node isoparametric finite element: nondimensional transverse displacement $\bar{u}_3 = 100 u_3 E_2 h^3 / q_0 a^4$ at the plate center.

			Mesh				
a/h	ℓ	Plate theory	4×4	6×6	8×8	Ref. [19]	Ref. [14]
10	0	$LW1$	0.740	0.740	0.740	0.740	0.715
		$LW2$	0.736	0.736	0.736	0.736	
		$LW3$	0.736	0.736	0.736	0.736	
		$LW4$	0.736	0.736	0.736	0.736	
	1	$LW1$	0.887	0.887	0.887	0.887	0.856
		$LW2$	0.881	0.881	0.881	0.881	
		$LW3$	0.881	0.881	0.881	0.881	
		$LW4$	0.881	0.881	0.881	0.881	
	3	$LW1$	1.179	1.179	1.179	1.179	1.139
		$LW2$	1.171	1.171	1.171	1.171	
		$LW3$	1.171	1.171	1.171	1.171	
		$LW4$	1.171	1.171	1.171	1.171	
	5	$LW1$	1.471	1.471	1.471	1.471	1.421
		$LW2$	1.462	1.462	1.462	1.462	
		$LW3$	1.462	1.462	1.462	1.462	
		$LW4$	1.462	1.462	1.462	1.462	
20	0	$LW1$	0.514	0.514	0.514	0.514	0.506
		$LW2$	0.513	0.513	0.513	0.513	
		$LW3$	0.513	0.513	0.513	0.513	
		$LW4$	0.513	0.513	0.513	0.513	
	1	$LW1$	0.615	0.615	0.615	0.615	0.606
		$LW2$	0.614	0.614	0.614	0.614	
		$LW3$	0.614	0.614	0.614	0.614	
		$LW4$	0.614	0.614	0.614	0.614	
	3	$LW1$	0.818	0.818	0.818	0.818	0.806
		$LW2$	0.816	0.816	0.816	0.816	
		$LW3$	0.816	0.816	0.816	0.816	
		$LW4$	0.816	0.816	0.816	0.816	
	5	$LW1$	1.021	1.021	1.021	1.021	1.006
		$LW2$	1.019	1.019	1.019	1.019	
		$LW3$	1.019	1.019	1.019	1.019	
		$LW4$	1.019	1.019	1.019	1.019	

accuracy. For the same plate and meshes, Figs. 4 and 5 show the through-the-thickness distributions

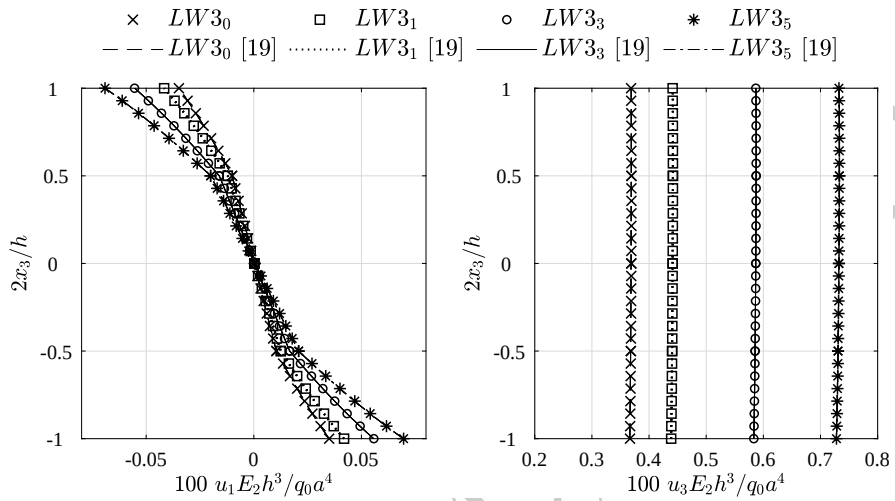

Figure 2: Through-the-thickness distribution of displacement components at the point of in-plane coordinates $(a/4,\ a/4)$ for the plate with $a/h = 10$. Results for the 8×8 regular mesh of 9-node isoparametric elements.

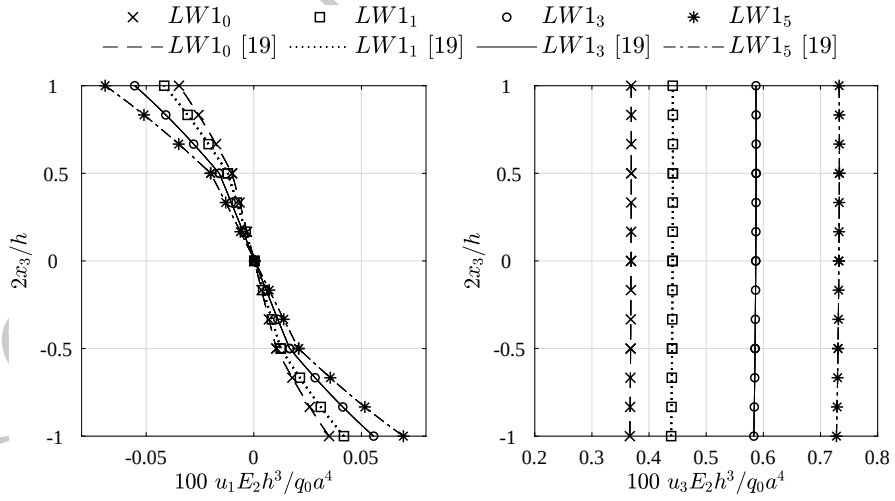

Figure 3: Through-the-thickness distribution of displacement components at the point of in-plane coordinates $(a/4,\ a/4)$ for the plate with $a/h = 10$. Results for the 5×5 regular mesh of 16-node isoparametric elements.

of the out-of-plane stresses σ_{13} and σ_{33} and their local counterparts $\widetilde{\sigma}_{13}$ and $\widetilde{\sigma}_{33}$. Firstly, it is observed

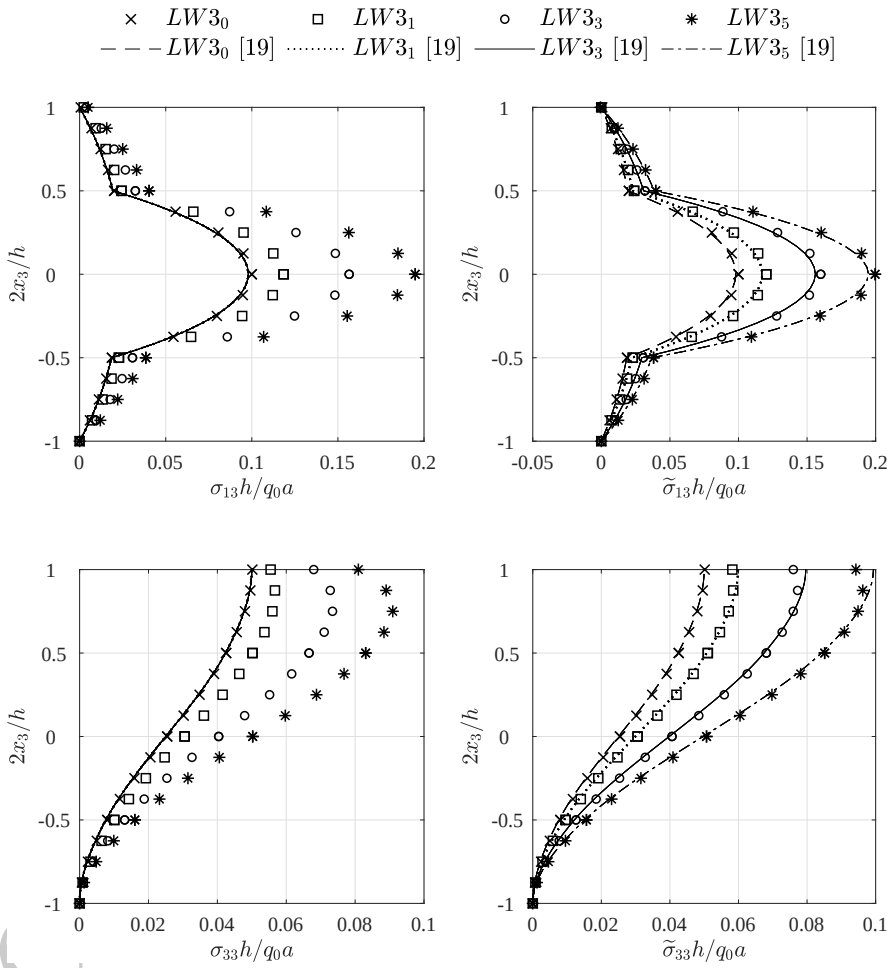

Figure 4: Through-the-thickness distribution of out of plane stress components at the point of in-plane coordinates $(a/4,\ a/4)$ for the plate with $a/h = 10$. Results for the 8×8 regular mesh of 9-node isoparametric elements.

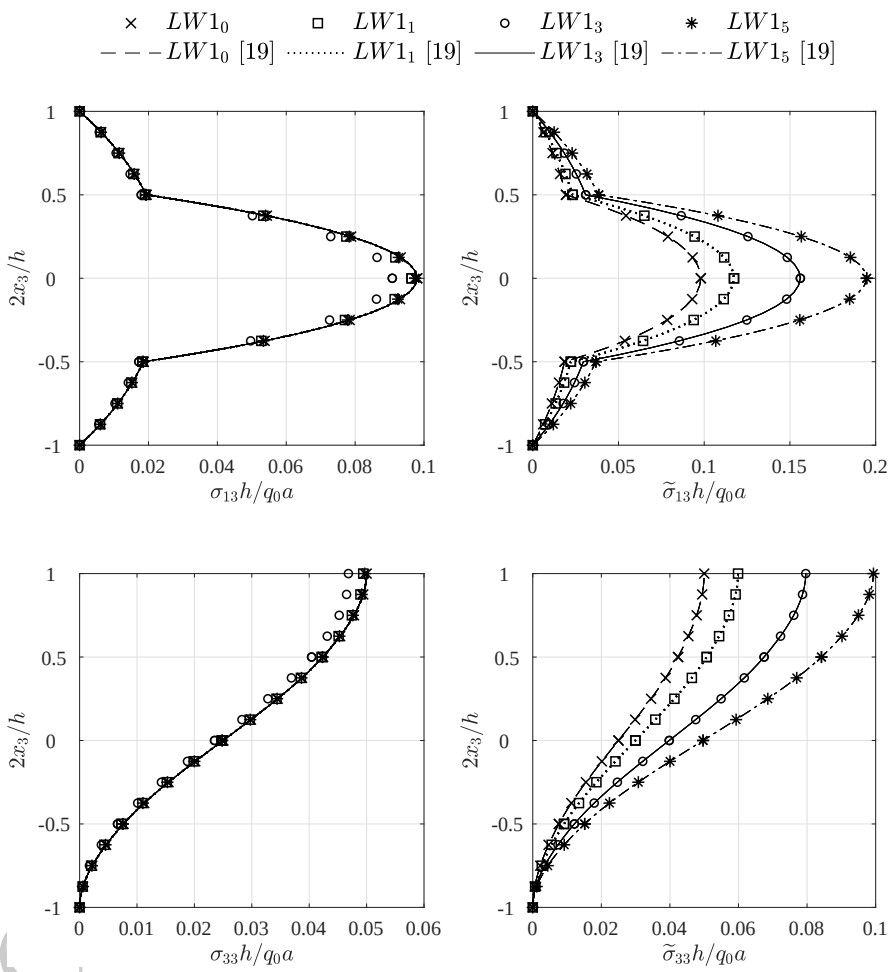

Figure 5: Through-the-thickness distribution of out of plane stress components at the point of in-plane coordinates $(a/4,\ a/4)$ for the plate with $a/h = 10$. Results for the 5×5 regular mesh of 16-node isoparametric elements.

that for both the element types very good agreement is achieved for the local stresses when compared to the closed form solution of Ref [19]. However, the examination of the non local stresses distributions for different values of the nonlocal parameter evidences that: (i) the 9-node element poorly represents the nonlocal stresses notwithstanding the local ones are accurate; (ii) the 16-node element exhibits a better behaviour in representing nonlocal stresses, which do not depend on the nonlocal parameter. Looking at the relationship between nonlocal and local stresses, namely Eqs. (1) and (2), this behaviour is attributed to the numerical approximation of the $\boldsymbol{\partial}_{\ell}^{\langle k \rangle}$ operator (matrix $\boldsymbol{\mathcal{H}}_{\eta}^{\langle k \rangle}$ in Eq. (10d)), which involves the second derivatives of the shape functions. Thus, it is reasoned out that in the framework of the isoparametric formulation higher order elements are required for reliable solutions.

In view of this remark it is argued that more effective finite elements could be formulated using improved approximations of the $\boldsymbol{\mathcal{H}}_{\eta}^{\langle k \rangle}$ operators. To this end, the concepts underlying assumed natural strains and mixed interpolation of tensorial components approaches can provide useful basis for the development of improved finite elements. However, this shall be considered out of the scope of the present work that aims to demonstrate the feasibility of the proposed approach.

As usual, a locking analysis was performed to verify that the use of the selective/reduced integration is able to manage this phenomenon. Tables 3 and 4 list the nondimensional transverse displacement $\overline{u}_3$ at the plate center for different thickness ratios a/h. and different nonlocal parameters ℓ. The present results have been obtained with 8×8 meshes of 9-node and 16-node elements, computing the involved matrices by using both full (FI) and selective reduced integration (SRI). The comparison of the results with the closed form solution of Ref. [19] evidences that very good accuracy can be obtained using selective/reduced integration both for thick and thin plates. The effects of the selective/reduced integration on the element's performances are further illustrated by the solution convergence curves. Figures 6 and 7 show the convergence features of the 9-node and 16-node elements based on the $LW3_5$ plate theory, respectively. In these figures, the percentage error of the transverse displacement at the plate central point versus the number of mesh elements curves is plotted for different plate thickness ($a/h = 10$ and $a/h = 1000$) and for both full and selective/reduced integration cases The plotted percentage error is computed with respect to the corresponding value obtained using the closed form solution given in Ref. [19]. It is worth noting that the reported convergence curves shall be considered as representative of a generalize behaviour; indeed, similar trends have been also found for elements based on different nonlocal plate theories and nonlocal parameters. The data prove the capability of the selective/reduced integration to contrast potential locking phenomena and improve

the solution accuracy. The proposed finite elements are employed to carry out original results for

Table 3: Locking analysis for the 9-node isoparametric finite element. Nondimensional transverse displacement $\bar{u}_3 = 100u_3E_2h^3/q_0a^4$ at the plate center computed with full (FI) and selective reduced (SRI) integration.

		$LW1$			$LW3$			$LW4$		
ℓ	a/h	FI	SRI	Ref. [19]	FI	SRI	Ref. [19]	FI	SRI	Ref. [19]
0	10	0.744	0.742	0.740	0.739	0.737	0.736	0.741	0.739	0.736
	100	0.437	0.435	0.435	0.437	0.435	0.435	0.437	0.437	0.435
	1000	0.434	0.431	0.431	0.434	0.431	0.431	0.433	0.433	0.431
1	10	0.890	0.887	0.887	0.885	0.881	0.881	0.886	0.885	0.881
	100	0.523	0.520	0.520	0.523	0.520	0.520	0.523	0.523	0.520
	1000	0.519	0.516	0.516	0.519	0.516	0.516	0.519	0.519	0.516
3	10	1.183	1.179	1.179	1.176	1.172	1.171	1.178	1.176	1.171
	100	0.696	0.692	0.692	0.695	0.692	0.692	0.696	0.695	0.692
	1000	0.690	0.687	0.687	0.690	0.687	0.687	0.690	0.690	0.687
5	10	1.477	1.471	1.471	1.468	1.462	1.462	1.470	1.468	1.462
	100	0.868	0.864	0.864	0.868	0.864	0.864	0.868	0.868	0.864
	1000	0.861	0.857	0.857	0.861	0.857	0.857	0.862	0.861	0.857

Table 4: Locking analysis for the 16-node isoparametric finite element. Nondimensional transverse displacement $\bar{u}_3 = 100u_3E_2h^3/q_0a^4$ at the plate center computed with full (FI) and selective reduced (SRI) integration.

		$LW1$			$LW3$			$LW4$		
ℓ	a/h	FI	SRI	Ref. [19]	FI	SRI	Ref. [19]	FI	SRI	Ref. [19]
0	10	0.740	0.740	0.740	0.736	0.736	0.736	0.736	0.736	0.736
	100	0.435	0.435	0.435	0.435	0.435	0.435	0.435	0.435	0.435
	1000	0.431	0.431	0.431	0.431	0.431	0.431	0.431	0.431	0.431
1	10	0.887	0.887	0.887	0.881	0.881	0.881	0.881	0.881	0.881
	100	0.520	0.520	0.520	0.520	0.520	0.520	0.520	0.520	0.520
	1000	0.517	0.516	0.516	0.517	0.516	0.516	0.517	0.516	0.516
3	10	1.179	1.179	1.179	1.171	1.171	1.171	1.171	1.171	1.171
	100	0.692	0.692	0.692	0.692	0.692	0.692	0.692	0.692	0.692
	1000	0.691	0.689	0.687	0.711	0.691	0.687	0.694	0.690	0.687
5	10	1.471	1.471	1.471	1.462	1.462	1.462	1.462	1.462	1.462
	100	0.864	0.864	0.864	0.864	0.864	0.864	0.864	0.864	0.864
	1000	0.859	0.852	0.857	0.852	0.852	0.857	0.852	0.852	0.857

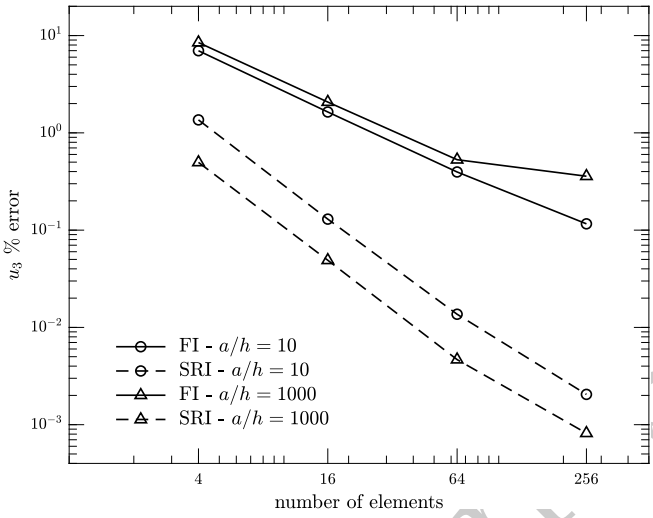

Figure 6: Convergence curves for the 9-node element based on the $LW3_5$ theory : percentage error of the central point transverse displacement $u_3(0.5L, 0.5L, 0)$ vs the number of elements.

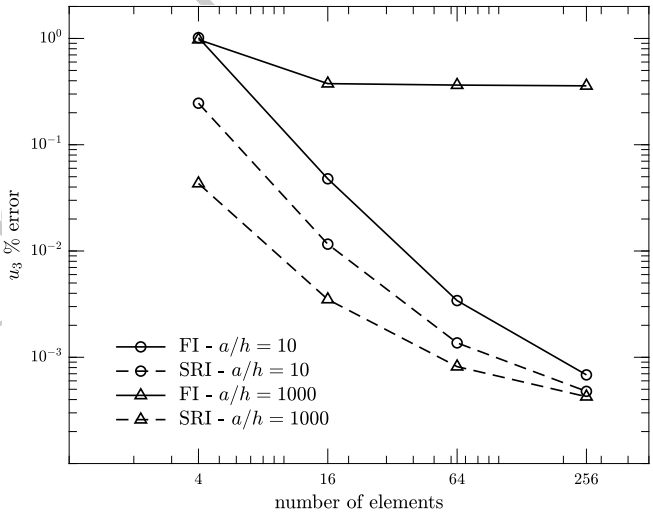

Figure 7: Convergence curves for the 16-node element based on the $LW3_5$ theory : percentage error of the central point transverse displacement $u_3(0.5L, 0.5L, 0)$ vs the number of elements.

a clamped, three-layered, square nanoplate with side length $a = 10$ nm. The plate external layers are graphene sheets with 0.34 nm thickness, modeled as nonlocal isotropic material with Young modulus $E_G = 1.6$ TPa and Poisson's ratio $\nu_G = 0.3$ [34]. The graphene nonlocal parameter is assumed varying in the range $\ell_G = 0.5 \div 1.5$ nm. The internal layer has thickness 0.34nm and is made of epoxy resin modeled as an isotropic material with Young modulus $E_E = 3.5$GPa and Poisson's ratio $\nu_E = 0.33$; local behaviour($\ell_E = 0$) is assumed for the epoxy resin. Fig. 8 shows the through-the-thickness distribution of displacement, stresses and local stresses at the point of in-plane coordinates ($a/3$, $a/3$). The presented solution has been obtained with the $LW3$ expansion. These original results aim to illustrate the formulation capability to deal with layers exhibiting different nonlocal parameter and to provide benchmarking data for the problem.

5. Conclusions

A novel mixed finite element formulation for the layerwise analysis of nonlocal multilayered composite plates has been presented. The formulation starting point is the weak form of the layers governing equations obtained via the Reissner Mixed Variational Theorem in which the displacements and out-of-plane stresses are assumed as primary variables. These primary variables are expressed at layer level as through-the-thickness expansions of suitable selected functions whose coefficients are approximated by the finite element scheme. The through-the-thickness expansion order is considered as a free parameter, so that different refined higher order plate theories are systematically developed. The contributions to the finite element equations associated with the variable expansion terms, the so-called fundamental nuclei, are firstly deduced for the laminate layers and then used in a layerwise assembly procedure to obtain the plate finite element matrices. The developed formulation inherently ensures the interface continuity. Moreover, it allows to consider different values of the nonlocal parameter for the layers.

To demonstrate the feasibility of the proposed formulation, 9-node and 16-node isoparametric, quadrilateral finite elements have been implemented and used to analyze plates by different order theories. The approach has been validated and its features assessed by comparison of the obtained results with closed-form solutions available in the literature. In the context of the isoparametric formulation, it is turned out the need to use higher order finite elements to capture reliably the nonlocal stress behaviour. This is related to the involvement in the formulation of the second order derivatives of the stresses that are poorly modeled by low order shape functions. The last observation suggests for

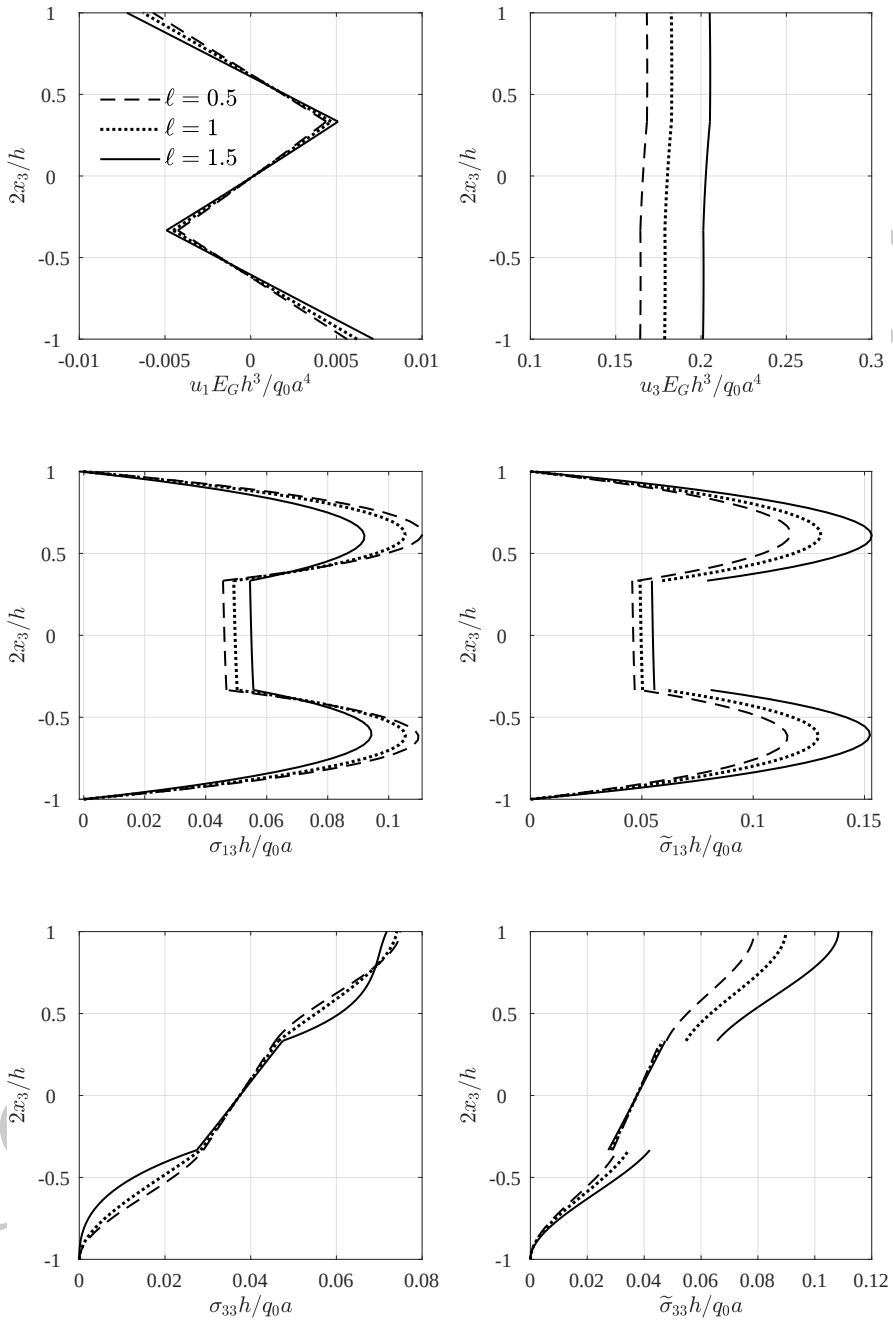

Figure 8: Through-the-thickness distribution of displacement components at the point of in-plane coordinates $(0.25L, 0.25L)$. 8×8 mesh of 16-node isoparametric elements

future alternative finite element formulations with improved approximation schemes for the primary variable second derivatives, for example exploiting the principles underlying the assumed natural strain and mixed interpolation of tensorial components approaches. Finally, original results have been also presented to better illustrate the proposed formulation potentiality and provide benchmarking data.

Acknowledgments

This work was partially supported by the Italian Ministry of Instruction, University and Reasearch (MIUR) through the project DEVISU in the funding scheme PRIN-2017 - grant 22017ZX9X4K_006.

Data availability statement

The data required to reproduce these findings cannot be shared at this time as they also form part of an ongoing study.

References

[1] K. F. Wang, B. L. Wang, T. Kitamura, A review on the application of modified continuum models in modeling and simulation of nanostructures, Acta Mechanica Sinica 32 (1) (2016) 83–100.

[2] H.-T. Thai, T. Vo, T.-K. Nguyen, S.-E. Kim, A review of continuum mechanics models for size-dependent analysis of beams and plates, Composite Structures 177 (2017) 196–219.

[3] A. Eringen, D. Edelen, On nonlocal elasticity, International Journal of Engineering Science 10 (3) (1972) 233 – 248.

[4] A. Eringen, On differential equations of nonlocal elasticity and solutions of screw dislocation and surface waves, Journal of Applied Physics 54 (9) (1983) 4703–4710.

[5] A. Eringen, Nonlocal Continuum Field Theories, Springer, 2002.

[6] R. Maranganti, P. Sharma, Length scales at which classical elasticity breaks down for various materials, Physical Review Letters 98 (19).

[7] J. Reddy, Nonlocal theories for bending, buckling and vibration of beams, International Journal of Engineering Science 45 (2-8) (2007) 288–307.

[8] J. Reddy, Nonlocal nonlinear formulations for bending of classical and shear deformation theories of beams and plates, International Journal of Engineering Science 48 (11) (2010) 1507–1518.

[9] P. Khodabakhshi, J. Reddy, A unified beam theory with strain gradient effect and the von Karman nonlinearity, ZAMM Zeitschrift fur Angewandte Mathematik und Mechanik 97 (1) (2017) 70–91.

[10] I. Mechab, N. E. Meiche, F. Bernard, Free vibration analysis of higher-order shear elasticity nanocomposite beams with consideration of nonlocal elasticity and Poisson effect, Journal of Nanomechanics and Micromechanics 6 (3) (2016) 04016006.

[11] P. Lu, P. Zhang, H. Lee, C. Wang, J. Reddy, Non-local elastic plate theories, Proceedings of the Royal Society A: Mathematical, Physical and Engineering Sciences 463 (2088) (2007) 3225–3240.

[12] R. Aghababaei, J. Reddy, Nonlocal third-order shear deformation plate theory with application to bending and vibration of plates, Journal of Sound and Vibration 326 (1-2) (2009) 277–289.

[13] P. Raghu, K. Preethi, A. Rajagopal, J. Reddy, Nonlocal third-order shear deformation theory for analysis of laminated plates considering surface stress effects, Composite Structures 139 (2016) 13–29.

[14] P. Raghu, A. Rajagopal, J. Reddy, Nonlocal nonlinear finite element analysis of composite plates using TSDT, Composite Structures 185 (2018) 38–50.

[15] A. Alaimo, M. Bruno, A. Milazzo, C. Orlando, Nonlocal model for a magneto-electro-elastic nanoplate, AIP Conference Proceedings 1558 (2013) 1208–1211.

[16] A. Farajpour, M. Hairi Yazdi, A. Rastgoo, M. Loghmani, M. Mohammadi, Nonlocal nonlinear plate model for large amplitude vibration of magneto-electro-elastic nanoplates, Composite Structures 140 (2016) 323–336.

[17] M. Mohammadimehr, R. Rostami, Bending, buckling, and forced vibration analyses of nonlocal nanocomposite microplate using TSDT considering MEE properties dependent to various volume fractions of $CoFe_2O_4 - BaTiO_3$, Journal of Theoretical and Applied Mechanics (Poland) 55 (3) (2017) 853–868.

[18] W. Park, S. Han, Buckling analysis of nano-scale magneto-electro-elastic plates using the nonlocal elasticity theory, Advances in Mechanical Engineering 10 (8).

[19] A. Milazzo, I. Benedetti, V. Gulizzi, Advanced models for nonlocal magneto-electro-elastic multilayered plates based on Reissner Mixed Variational Theorem, Mechanics of Advanced Materials and Structures 0 (0) (2019) 1–17. doi:10.1080/15376494.2019.1647480.

[20] E. Carrera, Theories and finite elements for multilayered plates and shells: A unified compact formulation with numerical assessment and benchmarking, Archives of Computational Methods in Engineering 10 (3) (2003) 215–296.

[21] E. Carrera, L. Demasi, Classical and advanced multilayered plate elements based upon PVD and RMVT. Part 1: Derivation of finite element matrices, International Journal for Numerical Methods in Engineering 55 (2) (2002) 191–231.

[22] J. Phadikar, S. Pradhan, Variational formulation and finite element analysis for nonlocal elastic nanobeams and nanoplates, Computational Materials Science 49 (3) (2010) 492–499.

[23] O. Polit, T. Merzouki, M. Ganapathi, Elastic stability of curved nanobeam based on higher-order shear deformation theory and nonlocal analysis by finite element approach, Finite Elements in Analysis and Design 146 (2018) 1–15.

[24] A. Aria, M. Friswell, A nonlocal finite element model for buckling and vibration of functionally graded nanobeams, Composites Part B: Engineering 166 (2019) 233–246.

[25] J. Sladek, V. Sladek, S. Hrcek, E. Pan, The nonlocal and gradient theories for a large deformation of piezoelectric nanoplates, Composite Structures 172 (2017) 119–129.

[26] K. Mehar, T. Mahapatra, S. Panda, P. Katariya, U. Tompe, Finite-element solution to nonlocal elasticity and scale effect on frequency behavior of shear deformable nanoplate structure, Journal of Engineering Mechanics 144 (9).

[27] P. Aurojyoti, P. Raghu, A. Rajagopal, J. Reddy, An n-sided polygonal finite element for nonlocal nonlinear analysis of plates and laminates, International Journal for Numerical Methods in Engineering 120 (9) (2019) 1071–1107.

[28] E. Reissner, On a certain mixed variational theorem and a proposed application, International Journal for Numerical Methods in Engineering 20 (7) (1984) 1366–1368.

[29] E. Reissner, On a mixed variational theorem and on shear deformable plate theory, International Journal for Numerical Methods in Engineering 23 (2) (1986) 193–198.

[30] E. Carrera, Developments, ideas, and evaluations based upon Reissner's Mixed Variational Theorem in the modeling of multilayered plates and shells, Applied Mechanics Reviews 54 (4) (2001) 301–328.

[31] I. Benedetti, A. Milazzo, Advanced models for smart multilayered plates based on Reissner Mixed Variational Theorem, Composites Part B: Engineering 119 (2017) 215–229.

[32] K. Bathe, Finite element procedures, Prentice Hall, 1996.

[33] D. Arnold, F. Brezzi, The partial selective reduced integration method and applications to shell problems, Computers and Structures 64 (1-4) (1997) 879–880.

[34] Q. Wang, Effective in-plane stiffness and bending rigidity of armchair and zigzag carbon nanotubes, International Journal of Solids and Structures 41 (20) (2004) 5451 – 5461.

Appendix A. Thickness functions

The thickness functions $F_r^{\langle k\rangle}$ are selected as a linear combination of Legendre polynomials $\mathcal{P}_i(\zeta_k)$ of i-th order as follows

$$F_0^{\langle k\rangle} = \frac{\mathcal{P}_0(\zeta_k) - \mathcal{P}_1(\zeta_k)}{2} \tag{A.1a}$$

$$F_r^{\langle k\rangle} = \mathcal{P}_{r+1}(\zeta_k) - \mathcal{P}_{r-1}(\zeta_k) \qquad r = 1, ...(M-1) \tag{A.1b}$$

$$F_M^{\langle k\rangle} = \frac{\mathcal{P}_0(\zeta_k) + \mathcal{P}_1(\zeta_k)}{2} \tag{A.1c}$$

where $\zeta_k = (2x_3 - z_k - z_{k-1}) / (z_k - z_{k-1})$ is the layer normalized thickness coordinate.

It is worth to remark that

$$F_r^{\langle k\rangle}(-1) = \begin{cases} 1 & \text{for } r = 0 \\ 0 & \text{for } r \neq 0 \end{cases} ; \tag{A.2a}$$

$$F_r^{\langle k\rangle}(1) = \begin{cases} 1 & \text{for } r = M \\ 0 & \text{for } r \neq M \end{cases} ; \tag{A.2b}$$

Appendix B. Definitions

The differential operators involved in the fundamental nuclei definitions, see Eqs.(7), are given by

$$\boldsymbol{\partial}_p = \begin{bmatrix} \dfrac{\partial}{\partial x_1} & 0 & 0 \\ 0 & \dfrac{\partial}{\partial x_2} & 0 \\ \dfrac{\partial}{\partial x_2} & \dfrac{\partial}{\partial x_1} & 0 \end{bmatrix} \tag{B.1a}$$

$$\boldsymbol{\partial}_n = \begin{bmatrix} 0 & 0 & \dfrac{\partial}{\partial x_1} \\ 0 & 0 & \dfrac{\partial}{\partial x_2} \\ 0 & 0 & 0 \end{bmatrix} \tag{B.1b}$$

$$\boldsymbol{\partial}_\ell^{\langle k \rangle} = \begin{bmatrix} \mathcal{L}^{\langle k \rangle} & 0 & 0 \\ 0 & \mathcal{L}^{\langle k \rangle} & 0 \\ 0 & 0 & \mathcal{L}^{\langle k \rangle} \end{bmatrix} \tag{B.1c}$$

Accordingly, the operators $\widehat{\boldsymbol{\partial}}_p$ and $\widehat{\boldsymbol{\partial}}_n$ are obtained from the differential operators $\boldsymbol{\partial}_p$ and $\boldsymbol{\partial}_n$ by substituting the partial derivatives with the corresponding boundary normal direction cosines. The layer constitutive matrices are defined as

$$\boldsymbol{D}_{pp}^{\langle k \rangle} = \boldsymbol{C}_{pp}^{\langle k \rangle} - \boldsymbol{C}_{pn}^{\langle k \rangle} {\boldsymbol{C}_{nn}^{\langle k \rangle}}^{-1} \boldsymbol{C}_{np}^{\langle k \rangle} \tag{B.2a}$$

$$\boldsymbol{D}_{pn}^{\langle k \rangle} = \boldsymbol{C}_{pn}^{\langle k \rangle} {\boldsymbol{C}_{nn}^{\langle k \rangle}}^{-1} \tag{B.2b}$$

$$\boldsymbol{D}_{np}^{\langle k \rangle} = -{\boldsymbol{C}_{nn}^{\langle k \rangle}}^{-1} \boldsymbol{C}_{np}^{\langle k \rangle} \tag{B.2c}$$

$$\boldsymbol{D}_{nn}^{\langle k \rangle} = {\boldsymbol{C}_{nn}^{\langle k \rangle}}^{-1} \tag{B.2d}$$

The coefficients $\mathcal{I}_{rs}^{\langle k \rangle}$ are

$$\langle \mathcal{I}_{rs}^{\langle k \rangle};\, \mathcal{I}_{r,3s}^{\langle k \rangle};\, \mathcal{I}_{rs,3}^{\langle k \rangle} \rangle = \int_{z_{k-1}}^{z_k} \langle F_r F_s;\, \frac{\partial F_r}{\partial x_3} F_s;\, F_r \frac{\partial F_s}{\partial x_3} \rangle dx_3 \tag{B.3}$$

Finally, the $\overline{\boldsymbol{p}}_\alpha$ terms are given by

$$\overline{\boldsymbol{p}}_\alpha = \int_{z_{k-1}}^{z_k} F_\alpha^{\langle k \rangle} \mathcal{L}\, \overline{\boldsymbol{t}}^{\langle k \rangle} dx_3 \tag{B.4}$$